Extracellular RNA Sensing Mediates Inflammation and Organ Injury in a Murine Model of Polytrauma

Andrew O. Suen,*,† Fengqian Chen,* Sheng Wang,* Ziyi Li,‡ Jing Zhu,* Yang Yang,* Olivia Conn,* Kerri Lopez,* Ping Cui,* Laurence Wechsler,* Alan Cross,§ Gary Fiskum,* Rosemary Kozar,* Peter Hu,* Catriona Miller,*,¶ Lin Zou,* Brittney Williams,* and Wei Chao*

Severe traumatic injury leads to marked systemic inflammation and multiorgan injury. Endogenous drivers such as extracellular nucleic acid may play a role in mediating innate immune response and the downstream pathogenesis. Here, we explored the role of plasma extracellular RNA (exRNA) and its sensing mechanism in inflammation and organ injury in a murine model of polytrauma. We found that severe polytrauma—bone fracture, muscle crush injury, and bowel ischemia—induced a marked increase in plasma exRNA, systemic inflammation, and multiorgan injury in mice. Plasma RNA profiling with RNA sequencing in mice and humans revealed a dominant presence of miRNAs and marked differential expression of numerous miRNAs after severe trauma. Plasma exRNA isolated from trauma mice induced a dose-dependent cytokine production in macrophages, which was almost abolished in TLR7-deficient cells but unchanged in TLR3-deficient cells. Moreover, RNase or specific miRNA inhibitors against the selected proinflammatory miRNAs (i.e., miR-7a-5p, miR-142, let-7j, miR-802, and miR-146a-5p) abolished or attenuated trauma plasma exRNA-induced cytokine production, respectively. Bioinformatic analyses of a group of miRNAs based on cytokine readouts revealed that high uridine abundance (>40%) is a reliable predictor in miRNA mimic-induced cytokine and complement production. Finally, compared with the wild-type, TLR7-knockout mice had attenuated plasma cytokine storm and reduced lung and hepatic injury after polytrauma. These data suggest that endogenous plasma exRNA of severely injured mice and ex-miRNAs with high uridine abundance prove to be highly proinflammatory. TLR7 sensing of plasma exRNA and ex-miRNAs activates innate immune responses and plays a role in inflammation and organ injury after trauma. ***The Journal of Immunology*****, 2023, 210: 1990–2000.**

Despite significant improvements in damage control resuscitation and care of seriously injured patients, severe traumatic injury is still a leading cause of death in persons younger than 50 y of age and directly impacts over 35,000 soldiers wounded in action in recent conflicts (1–3). Immediate effects of trauma include the direct and indirect mechanical forces acting on tissues, which in turn induces local tissue damage, contusions, hemorrhage, fractures, and compromised host defense mechanisms due to disrupted barrier defenses (4–6). Subsequently, immunological and inflammatory responses frequently follow severe traumatic injury and are, in part, a consequence of innate immune activation by endogenous drivers (7–9).

The innate immune system functions to detect and defend against threats to its host by triggering an inflammatory response against pathogen- or damage-associated alarm signals using a ubiquitous set of conserved pattern recognition receptors (PRRs) located on cells of the innate immune system (10). These PRRs serve to sense molecular structures known as pathogen- or damage-associated molecular patterns released by invading pathogens or host cells and tissues, respectively (11, 12). One such family of PRRs, the TLRs, is a prominent group of sensors that recognize various pathogen components, such as LPS and lipoproteins, and endogenous danger molecules, such as HMGB-1, histone, and nucleic acid. When engaged with their respective ligands, TLRs activate downstream signaling pathways and promote the production of inflammatory mediators and activation of innate immune cells. Among multiple TLRs that serve to sense nucleic acids (11, 12), TLR7 is known as the sensor for ssRNAs, such as those found in viral particles (13). Critically, its endosomal localization is thought to prevent recognition of self-derived RNA ligands (14, 15), given the ubiquitous presence of RNA.

It has been postulated that the release of various nucleic acids into the circulation following tissue injury drives proinflammatory

*Center for Shock, Trauma and Anesthesiology Research, University of Maryland School of Medicine, Baltimore, MD; †Department of Anesthesia, Pain Management & Perioperative Medicine, Dalhousie University, Halifax, NS, Canada; ‡Department of Biostatistics, The University of Texas MD Anderson Cancer Center, Houston, TX; §Department of Medicine, University of Maryland School of Medicine, Baltimore, MD; and ¶Enroute Care Division, Department of Aeromedical Research, U.S. Air Force School of Aerospace Medicine, Wright Patterson Air Force Base, Dayton, OH

ORCIDs: 0000-0002-4354-6498 (A.O.S.); 0000-0001-8359-0533 (Z.L.); 0000-0003-4362-9936 (A.C.); 0000-0001-5909-0539 (G.F.); 0000-0002-9198-7351 (R.K.); 0000-0002-7243-8058 (C.M.); 0000-0003-0820-4246 (L.Z.); 0000-0002-2505-1360 (W.C.).

Received for publication February 8, 2023. Accepted for publication April 6, 2023.

This work was supported in part by the U.S. Air Force Research Laboratory Grants FA8650-17-2-6HJ12 (W.C. and C.M.) and FA8650-18-2-6H17 (G.F., W.C., and A.C.); National Institutes of Health Grants R01-GM117233/R01-GM122908/R35-GM140822 (W.C.), R35-GM124775 (L.Z.), and K08-HL153784 (B.W.); and a Dalhousie University, Department of Anesthesia, and Nova Scotia Ministry of Health Research Training Grant (A.O.S.).

The small RNA sequencing data presented in this article have been submitted to the National Center for Biotechnology Information Gene Expression Omnibus (https://www.ncbi.nlm.nih.gov/geo/query/acc.cgi?acc=GSE223151) under accession number GSE223151.

A part of this work was reported previously in abstract form at the 41 Annual Conference on SHOCK, June 9–12, 2018, Scottsdale, AZ (*Shock* 2018; 49: 45).

Address correspondence and reprint requests to Dr. Lin Zou and Dr. Brittney Williams and Dr. Wei Chao, Center for Shock, Trauma and Anesthesiology Research, University of Maryland School of Medicine, S003, HSF-2, 20 Penn Street, Baltimore, MD 21201. E-mail addresses: lzou@som.umaryland.edu (L.Z.) and brittney.williams@som.umaryland.edu (B.W.) and wchao@som.umaryland.edu (W.C.)

The online version of this article contains supplemental material.

Abbreviations used in this article: AST, aspartate aminotransferase; BAL, bronchoalveolar lavage; BMDM, bone marrow-derived macrophage; cfB, complement factor B; CO, cardiac output; exRNA, extracellular RNA; KO, knockout; LVIDd, left ventricular internal diameter at the end of diastole; LVIDs, left ventricular internal diameter at the end of systole; PRR, pattern recognition receptor; RNAseq, RNA sequencing; ROC, receiver operating characteristic; SAX, short axis; SMA, superior mesenteric artery; WT, wild-type.

immune responses through the triggering of sensing pathways (11). As a result, the potential role of extracellular nucleic acids after tissue injury has previously been explored, such as mitochondrial DNA (16) and microRNAs (miRNAs) as potential biomarkers of traumatic injury (17–19). These miRNAs, a group of small noncoding ssRNAs 20–24 nt in length, are considered to function primarily intracellularly in post-transcriptional gene regulation by binding to the 3′ untranslated region of target mRNAs. Importantly, miRNAs have also been found in a wide range of body fluids of healthy volunteers (20) and in the critically injured (19). We have recently reported that host cellular miRNAs are released into the circulation during sepsis (21, 22) and myocardial ischemic injury (23). We found that certain miRNAs have a unique capability to induce a proinflammatory response through a TLR7-dependent mechanism (22, 23).

Although extracellular (ex)-miRNAs have been implicated in several diseases, including trauma (18) and sepsis (22, 24, 25), the expression patterns of circulating plasma ex-miRNAs after traumatic injury and their biological roles and mechanisms in trauma-induced inflammation and injury remain unclear. Here, we tested the hypothesis that traumatic injury induces a release of endogenous cellular RNAs that are potent activators of innate immunity and injury-induced inflammation. To test this, we established a mouse model of polytrauma and performed RNA sequencing (RNAseq) to profile plasma extracellular RNA (exRNA) in healthy and severely injured animals and humans. We examined the role of plasma exRNA and its signaling pathway in innate immune activation and organ injury after trauma.

Materials and Methods

Human subjects

Healthy volunteers and trauma patients were enrolled under the protocol (HP-00079925) approved by the institutional review board of the University of Maryland School of Medicine and by the Air Force Surgeon General Office of Research Oversight and Compliance. Trauma patients aged 18 y or older with nonpenetrating blunt trauma to the extremities, chest, abdomen, and pelvis and with injuries to bone, lung, spleen, liver, bowel, kidney, and aorta were enrolled upon arrival at the Shock Trauma Center, University of Maryland at Baltimore. Age- and sex-matched healthy control subjects were enrolled at the General Clinical Research Center of the University of Maryland Medical Center. The detailed demographic and clinical data of both trauma and control cohorts are listed in Table I. Both trauma and healthy subjects were enrolled with written informed consent and based on the institutional review board–approved inclusion and exclusion criteria. Plasma was prepared from blood samples by centrifugation (1,000 × *g* for 10 min twice followed by 10,000 × *g* for 10 min at 4°C). All studies involving human subjects were conducted in accordance with the guidelines of the World Medical Association's Declaration of Helsinki.

Animal subjects

Eight- to 12-wk-old sex- and age-matched wild-type (WT) C57BL/6J mice were purchased from The Jackson Laboratory (Bar Harbor, ME). TLR3$^{-/-}$ (Tlr3^{tm1Flv}/J, stock no. 005217) and TLR7$^{-/-}$ (Tlr7^{tm1Flv}/J, stock no. 008380) mice were originally purchased from The Jackson Laboratory and have been bred in-house with C57BL/6J mice for more than 10 generations. All animals were housed for at least 1 wk before experiments in an air-conditioned, pathogen-free environment with free access to water and a bacteria-free diet at the animal veterinary facilities at the University of Maryland School of Medicine. Blinding and randomization were conducted using simple sequential numbering generated manually to determine group assignment. All animal care and procedures were reviewed and approved by the institutional animal care and use committee of the University of Maryland School of Medicine. All animal studies complied with the U.S. Department of Health and Human Services Guide for the Care and Use of Laboratory Animals. Institutional animal care and use committee protocols were also approved by Air Force Surgeon General Office of Research Oversight and Compliance.

Murine model of polytrauma

A polytrauma model was created consisting of bowel ischemia, bone fracture, and muscle crush, simulating combat injuries such as those induced by improvised explosive devices. Male mice were anesthetized using isoflurane (2.5% for induction, 2% for maintenance) with a fraction of inspired oxygen of 95–97% at a flow rate of 100 ml/min. After midline laparotomy, the superior mesenteric artery (SMA) was exposed via a perihepatic approach and occluded at the aortic origin using a microvascular clip. Bowel ischemia was confirmed visually by pallor in the distal bowel (Supplemental Fig. 1A), hypoperistalsis, and the absence of distal pulsating flow. The abdominal contents were replaced, and the abdominal wall was temporarily closed using Steri-Strips (3M) to minimize evaporative losses. At the end of 35 min of bowel ischemia, the SMA was partially exposed, and reperfusion was initiated by removal of the surgical clip and confirmed by the plethoric appearance of bowel, indicating restoration of perfusion. At the onset of SMA occlusion, a unilateral midshaft tibial fracture was induced by blunt force, and the ipsilateral gastrocnemius muscle was crushed by application of a Kelly forceps for 30 min. Reduction and external fixation of the fracture were performed using tape splinting and a hollow foam boot cast (Supplemental Fig. 1B). Sham animals underwent laparotomy and exposure of the SMA only. Fascial and skin layers were closed with running suture at the end of the sham or polytrauma procedure, and bupivacaine (3.5 mg/kg) was infiltrated widely at the incision. All animals were maintained at a rectal temperature of 36°C–37°C during all procedures using a homeothermic heating pad and were administered preemptive buprenorphine analgesia (0.1 mg/kg) and fluid supplementation (20 ml/kg) prior to instrumentation. Core rectal temperature was measured by a thermometer at different time points after procedures. Simple randomization was used to assign animals, and the operators (A.S., F.C.) were blinded to the mouse strain information.

Mouse blood and solid tissue sample collection

Animals were euthanized at 6 h and 24 h following polytrauma or sham procedure by cardiac puncture under general anesthesia. Blood samples were collected in K2EDTA phlebotomy tubes (MiniCollect, Greiner Bio-One) and immediately processed by two-step centrifugation at 1,000 × *g* and 10,000 × *g* for 10 min at 4°C to obtain a cell-free plasma aliquot, which was stored at −80°C in a freezer until further analysis. Tissues and thoracic and abdominal organ samples were collected sterilely and rinsed in cold PBS. Samples were immediately snap frozen in liquid nitrogen and stored at −80°C until further analysis.

Tissue histology

Kidney, liver, and skeletal muscle samples were collected, rinsed in PBS, and immersed in 10% neutral-buffered formalin for 24–48 h. Small bowel segments were first flushed with PBS to remove all luminal contents prior to immersion in neutral-buffered formalin. All specimens were subsequently embedded in paraffin, and 4-μm sections were stained with standard H&E by the histology core of the University of Maryland School of Medicine.

Measurement of plasma cytokines and organ injury serum markers

Plasma IL-6, TNF-α, and MIP-2 were tested using ELISA kits (R&D Systems). Myoglobin concentration was determined by ELISA (Life Diagnostics). Aspartate aminotransferase (AST) activity was measured by colorimetric enzyme activity assay kits (Sigma-Aldrich).

Mouse echocardiography

Mouse echocardiography was performed using a Vevo 2100 (FUJIFILM VisualSonics) under light sedation (ketamine 20 mg/kg i.p.) at 6 h and 24 h following the surgical procedures. Both B- and M-mode images were obtained with parasternal short-axis (SAX) and long-axis views. Image analysis was performed offline using Vevo Lab PC software (FUJIFILM VisualSonics). Left ventricular internal diameter at the end of diastole (LVIDd) and at the end of systole (LVIDs) were measured from SAX images obtained at the level of the papillary muscles. Stroke volume was determined by the change in LV cavity area between systole and diastole based on LV tracings of SAX and long-axis images, and ejection fraction was calculated as (end diastolic volume − end systolic volume)/end diastolic volume. Cardiac output (CO) and fractional shortening were calculated as heart rate × stroke volume, and (LVIDd − LVIDs)/LVIDd, respectively.

RNA extraction and quantification

RNA was extracted from homogenized tissues using TRIzol (Sigma-Aldrich) reagent according to the manufacturer's protocol, and concentration was measured using a NanoDrop One ultraviolet spectrophotometer (Thermo Fisher Scientific). For mouse plasma RNA extraction, TRIzol LS (Thermo Fisher Scientific) reagent was mixed with 50 μl of plasma samples along

with 9.9 amol of *Caenorhabditis elegans* mir-39 (Qiagen) as a spike-in control and processed according to the manufacturer's protocol. To improve RNA recovery yield, 5 μg of glycogen (Invitrogen) was added to samples during alcohol precipitation and chilled at −20°C for 18 h. For human plasma RNA extraction, a miRNeasy serum/plasma advanced kit (Qiagen) was used to extract RNA from 250 μl EDTA anticoagulated plasma following the manufacturer's instructions. The purified RNA pellets were then resuspended in diethyl pyrocarbonate–treated H_2O and quantified with the fluorometric Quant-iT RNA Assay Kit (Thermo Fisher Scientific). Alternatively, the Bioanalyzer 2100 Small RNA Kit (Agilent Technologies, Santa Clara, CA) was used to quantify small RNA.

Quantitative RT-PCR

For gene expression in solid tissues and cells, moloney murine leukemia virus reverse transcriptase (Promega) was used to synthesize cDNA from purified template RNA samples. Subsequently, quantitative real-time PCR with GoTaq Master Mix (Promega) was carried out in a QuantStudio 5 PCR thermocycler (Applied Biosystems). Relative expression of mRNA was calculated using the comparative cycle threshold method normalized to GAPDH expression. Sequences of 5′-3′ for the primers are as follows: mKIM-1 (kidney injury molecule-1), forward: 5′-CATTTAGGCCTATACT GC, reverse: 5′-CAAGCAGAAGATGGGCATT-3′; mNGAL, forward: 5′-CTCAGAACTTGATCCCTGCC-3′, reverse: 5′-TCCTTGAGGCCCAGA-GACTT-3′; mGAPDH, forward: 5′-AACTTTGGCATTGTGGAAGG-3′, reverse: 5′-GGATGCAGGGATGATGTTCT-3′; mIL-1β, forward: 5′-GCC CATCCTCTGTGACTCAT-3′, reverse: 5′-AGGCCACAGGTATTTTGTCG-3′; mIL-6, forward: 5′-AGTTGCCTTCTTGGGACTGA-3′, reverse: 5′-TCCAC-GATTTCCCAGAGAAC-3′; mTNF-α, forward: 5′-CTGGGACAGTGACC TGGACT-3′, reverse: 5′-GCACCTCAGGGAAGAGTCTG-3′.

RNAseq and bioinformatic analysis

Plasma RNA from mice and humans were used for small RNAseq library preparation. Libraries were sequenced on an Illumina NextSeq 500 (Illumina, San Diego, CA) and analyzed by Norgen Biotek Corp. The raw sequence data were analyzed using the exceRpt small RNAseq pipeline (Genboree Bioinformatics). Differential expression analysis was performed using R package edgeR version 3.24.0, which incorporates empirical Bayes estimation into a negative binomial distribution (26). The $\log_2$ fold change and log p values from differential expression analysis were used to draw heatmaps using the R package pheatmap version 1.0.12 (27). Target genes for selected miRNAs were predicted using the R package multiMiR (28), and functional analysis on these predicted targets was performed using the R package clusterProfiler version 4.4.4 (29). The small RNAseq data of the present study have been deposited in the National Center for Biotechnology Information Gene Expression Omnibus (GEO) and are accessible through GEO series accession number GSE223151 at https://www.ncbi.nlm.nih.gov/geo/query/acc.cgi?acc=GSE223151.

Cell culture and reagents

Bone marrow-derived macrophages (BMDMs). Cells were isolated from bone marrow flushed from the femurs and tibias of 8- to 12-wk-old male or female mice and cultured in the presence of M-CSF (R&D Systems). Cells were resuspended in RPMI 1640 growth medium supplemented with 10% FBS, 5% horse serum, and penicillin/streptomycin (100 U/ml) and seeded at a density of 2×10^6/ml on 6-well, 12-well, 24-well, or 96-well plates (3 ml/well, 2 ml/well, 0.5 ml/well, or 0.1 ml/well, respectively) in an incubator at 37°C with 5% CO_2. Growth medium was replaced 48 h after initial plating, and at 72 h, BMDMs were ~70–80% confluent and ready for experiments.

miRNAs. miRNA mimics were ordered from Integrated DNA Technologies as lyophilized ssRNAs with phosphorothioate internucleotidic linkages synthesized and purified by HPLC. ssRNAs were resuspended in sterile DNase-/RNase-free diethyl pyrocarbonate–treated H_2O and diluted to working concentrations.

Cell treatments. 1) miRNA mimics and TLRs ligand treatment. BMDMs were serum starved for 1 h prior to cell treatment by replacing growth medium with RPMI 1640 supplemented with 0.05% BSA. Synthetic miRNA mimics were complexed with Lipofectamine 3000 transfection reagent (Thermo Fisher Scientific) and incubated for 15 min at room temperature prior to addition of the RNA–lipid complex to cells. Lipofectamine, polyinosinic:polycytidylic acid (10 μg/ml; Enzo Life Sciences), R837 (1 μg/ml; InvivoGen), or Pam3Cys (1 μg/ml; Enzo Life Sciences) was added directly to wells. 2) Plasma RNA treatment. Various concentrations of plasma RNA isolated from sham or trauma mice 6 h after procedures were incubated with BMDMs, and media were collected 18 h later for ELISA or Western blot analysis. 3) RNase, DNase, and anti-miRNA treatment. Plasma RNA (0.25 μg/ml) from sham or trauma mice was also incubated with RNase A (10 μg; Sigma-Aldrich) or DNase (1 U; Thermo Scientific) at room temperature for 30 min before being packed with Lipofectamine 3000. To test the role of specific miRNAs in plasma RNA, locked nucleic acid miRNA inhibitors (Qiagen) were applied. BMDMs were pretreated with anti-miR-7a, anti-mi-142, anti-let7j, anti-miR-802, or anti-miR-146a at 50 nM or combined mixture at 250 nM for 1 h prior to treatment with plasma RNA at 0.25 μg/ml.

Western blot of complement factor B (cfB)

Proteins from equal volumes of cell culture medium were separated in a 4–20% gradient Tris-HCl SDS-PAGE (Bio-Rad Laboratories), transferred to polyvinylidene difluoride membranes, and immunoblotted overnight at 4°C with goat anti-human cfB Ab (1:2500 dilution, Complement Technology) in 5% nonfat dry milk as we reported before (30).

Bronchoalveolar lavage (BAL) collection

BAL fluid was collected from euthanized mice after instillation and aspiration of 1 ml Dulbecco's PBS into the trachea using a syringe. The procedure was repeated once. The collected BAL was centrifuged, and the supernatant was stored at −80°C.

Lung permeability assay

Lung permeability was evaluated using pulmonary leakage of a fluorescent dextran from the circulation as we reported recently (24). FITC-dextran (40 kDa, 2.5 mg/ml; Sigma-Aldrich) was delivered via the tail vein in a volume of 250 μl at 5.5 h after sham or trauma procedures. After 30 min, BAL and plasma were collected, and mean fluorescence intensity was measured using a fluorescent plate reader. The ratio of mean fluorescence intensity of BAL to plasma was used to reflect lung permeability.

Protein quantification assay

Protein was quantified using a bicinchoninic acid assay kit (Thermo Fisher Scientific) with the BAL collected as described above.

Plasma creatinine

Plasma creatinine was measured using the QuantiChrom creatinine assay kit from BioAssay Systems following the manufacturer's instructions.

Lung digestion and flow cytometry analysis

Mice were euthanized at 6 h after sham or trauma procedures, and their lungs were perfused through the right ventricle with 10 ml of PBS. The lungs were moved, cut into small pieces with scissors, transferred into C-tubes (Miltenyi Biotec, Auburn, CA), and processed in digestion buffer (1 mg/ml of collagenase D and 0.1 mg/ml DNase I, both from Roche) with a GentleMACS dissociator (Miltenyi Biotec) according to the manufacturer's instructions. Homogenized lungs were passed through a 40-μm cell strainer to obtain a single-cell suspension. The remaining RBCs were lysed using RBC lysis buffer (Thermo Fisher Scientific). The isolated cells were stained with viability dye of Zombie red (1:500, BioLegend) for 10 min on ice. The cells were washed and incubated with CD16/CD32 Fc blocker (0.5 μg/sample, Thermo Fisher Scientific) on ice for 10 min prior to staining with the following Abs: CD11b-Alexa Fluor 700A (BioLegend) and Ly6G-Percp-Cy5.5A (BioLegend) at 4°C for 30 min. The cells were then washed in PBS solution containing 5% FBS. Data were acquired on a Cytek Aurora (Cytek Bioscience) flow cytometer and analyzed by FlowJo (BD Biosciences). The leukocyte gating strategy is shown in Supplemental Fig. 2.

Statistical analysis

Continuous variables were expressed as the mean ± SEM for normally distributed data and median (25th, 75th percentiles) for nonnormal distributions. Categorical data are described or presented as count (percent). For two-group comparison, the Student t test or Mann-Whitney U test is applied. For multiple-group comparison, one-way ANOVA with Tukey post hoc test or two-way ANOVA with Bonferroni post hoc correction was applied when the data met the two assumptions normal population distribution and equal variance. If the data did not meet the assumptions, we performed ANOVA after the data were transformed to the log format, or we performed the Kruskal-Wallis test. The Mantel-Cox test was used for survival curve analysis. Receiver operating characteristic (ROC) curves were constructed to assess the sensitivity and specificity of four-nucleotide abundance and compare their ability to determine the inflammatory property. Analyses were performed using GraphPad Prism 6 (GraphPad Software, La Jolla, CA). Differences were considered significant at $p < 0.05$ with two tails.

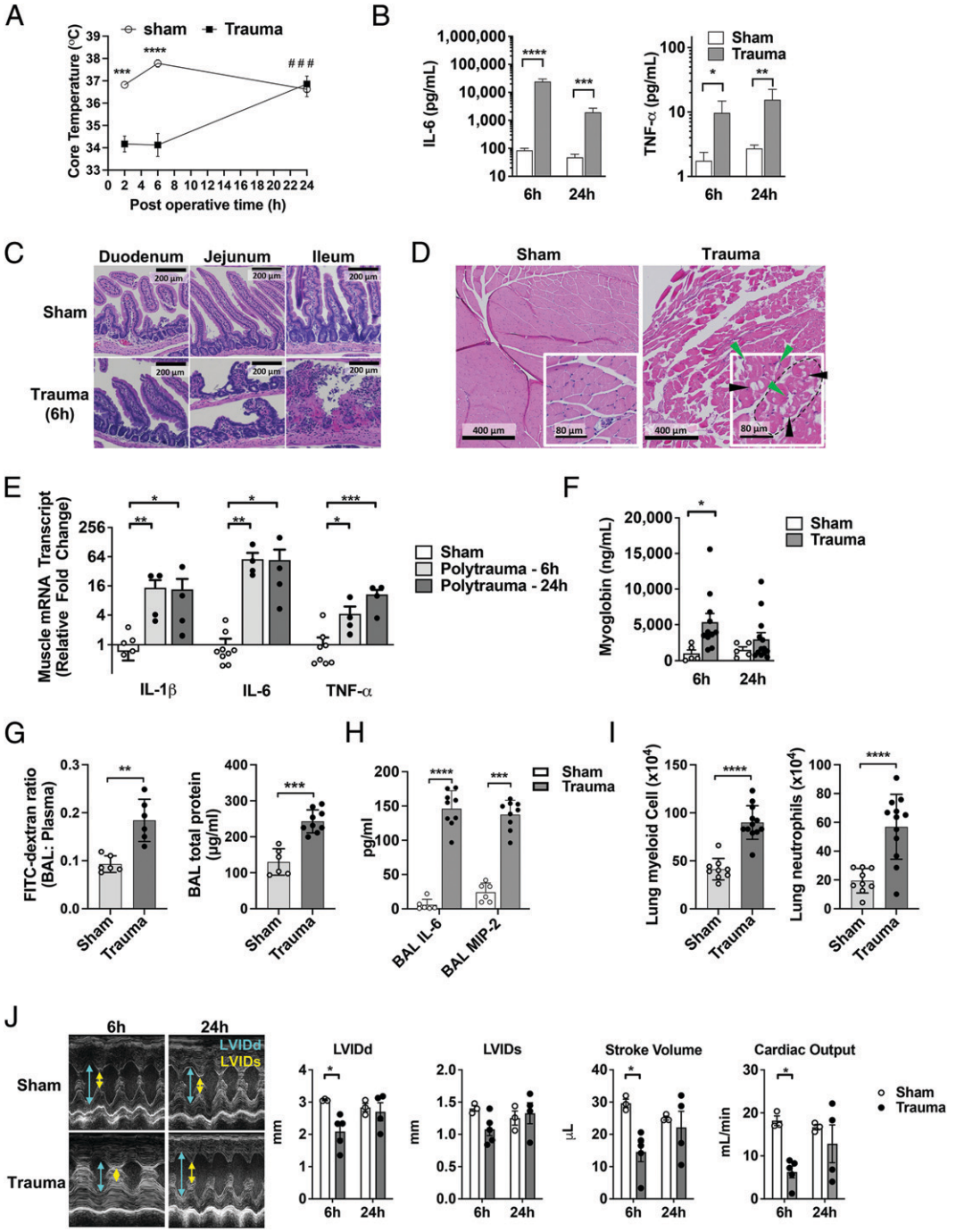

FIGURE 1. Polytrauma induces hypothermia, systemic inflammation, local tissue damage, and remote organ injury in mice. Mice were subjected to sham or polytrauma procedures as described in the *Materials and Methods* section. (**A**) Rectal core temperature. $^{***}p < 0.001$, $^{****}p < 0.0001$ versus trauma at the same time point. $^{\#\#\#}p < 0.001$ versus trauma 2 h and trauma 6 h. (**B**) Cytokine storm after traumatic injury. Six hours and 24 h after trauma or sham surgical procedures, mice were euthanized, and plasma was collected. Plasma IL-6 and TNF-α were analyzed by ELISA; $n = 5–7$. $^{*}p < 0.05$, $^{**}p < 0.01$, $^{***}p < 0.001$, $^{****}p < 0.0001$. (**C**) H&E staining of small bowels of trauma and sham mice. Six hours after the procedure, small bowels were collected, fixed, and stained with H&E. There are inflammatory cell infiltration, separation of the epithelium and the luminal basal layers, villous blunting, and near-complete disintegration of epithelial layers; sham mice display no observable mucosal damage. (**D**) Muscle injury. Crush injury of gastrocnemius muscle results in loss of organized muscle fascicular architecture (dotted line), severe intracellular vacuolization (black arrows), and global disruptions of muscle fiber membrane (green arrows). (**E**) Cytokine gene expression in gastrocnemius muscles 6 h after procedures. $^{*}p < 0.05$, $^{**}p < 0.01$, $^{***}p < 0.001$. $n = 4–9$. (**F**) Plasma myoglobin in sham and trauma mice. There is a rise in plasma myoglobin levels at 6 h as a consequence of traumatic rhabdomyolysis. $^{*}p < 0.05$, $n = 5–11$. (**G**) Lung permeability at 6 h after procedures. Alveolar-capillary permeability was measured by leakage of FITC-dextran (40 kDa) from blood circulation to alveolar space presented as the ratio of FITC fluorescence in BAL to plasma. BAL protein level was measured by bicinchoninic acid assay. $n = 6–9$/group. $^{**}p < 0.01$, $^{***}p < 0.001$ versus sham. (**H**) IL-6 and MIP-2 in the BAL at 6 h after sham or trauma. $^{***}p < 0.001$, $^{****}p < 0.0001$, $n = 6–9$/group. (**I**) Lung myeloid cells and neutrophil counts 6 h after procedures. $^{****}p < 0.0001$, $n = 6–9$/group. (**J**) Representative pictures of M-mode mouse echocardiography and quantitative values of LVIDd, LVIDs, stroke volume, and CO. $^{*}p < 0.05$, $n = 3–5$/group. Each data point represents an animal subject (original magnification ×20).

Results

Polytrauma induces marked local and systemic inflammation and multiple-organ injury

We established a murine polytrauma model (Supplemental Fig. 1A, 1B) with the three components, bowel ischemia, bone fracture, and muscle crush, a type of injury often occurring after improvised explosion, and we systematically examined inflammation and local and remote organ injury. Polytrauma mice initially exhibited a lower core temperature at 2 and 6 h after the procedure but recovered at 24 h (Fig. 1A). Polytrauma also led to a marked increase in plasma IL-6 and TNF-α levels at both 6 and 24 h (Fig. 1B). Histology confirmed severe bowel injury as evidenced by widespread intestinal mucosal damage, including severe villous blunting, marked neutrophil infiltration, and patchy mural necrosis with sloughing of the mucosa (Fig. 1C). Tibial fracture and muscle crush resulted in local muscle interstitial edema and necrosis (Fig. 1D); marked increases in muscle tissue inflammatory cytokine genes such as IL-1β, IL-6, and TNF-α (Fig. 1E); and a rise in plasma myoglobin at 6 h (Fig. 1F). The polytrauma model also resulted in multiple remote organ dysfunction and injury, such as the lung and heart. Marked acute lung injury was evidenced by increased lung permeability, alveolar cytokine production, and leukocyte infiltration at 6 h following polytrauma (Fig. 1G–1I). Echocardiography showed that 6 h after trauma, there was a decrease in both LVIDd and LVIDs, indicating ventricular hypovolemia (Fig. 1J). The stroke volume and CO were also decreased significantly at 6 h, with subsequent return to normal range by 24 h (Fig. 1J). Moreover, the average calculated ejection factions for sham and trauma mice were 82.9 ± 4.4% and 70.0 ± 11.0%, respectively, showing a statistically nonsignificant reduction of 12.9%. There was also significant acute kidney injury at 6 h, as demonstrated by increases in the acute kidney injury biomarkers KIM-1 and NGAL (neutrophil gelatinase-associated lipocalin) gene expression in the kidney, increases in plasma creatinine, and acute tubular necrosis (Supplemental Fig. 1C), as well as acute hepatic injury, as evidenced by increased AST and bile duct proliferation on histology (Supplemental Fig. 1D).

Traumatic injury leads to an increase in plasma exRNAs and differential expression of ex-miRNAs in mice and humans

Using high-resolution automated microelectrophoresis (Bioanalyzer 2100) (Fig. 2A), we observed a rise in small RNAs between 10 and 150 nt in size (112 ± 27 versus 399 ± 45 ng/ml; $p < 0.001$) in the mouse plasma 6 h after polytrauma (Fig. 2B). To profile plasma RNA, we performed RNAseq analysis of mouse and human plasma samples. In both mice (sham, $n = 6$; trauma, $n = 9$) and humans (healthy control, $n = 10$, trauma, $n = 10$, details in Table I), there was a marked increase in plasma RNA reads following trauma, and the predominant circulating plasma RNA—more than 80%—were miRNAs; the rest were rRNA, mRNA, piwi-interacting RNA, and tRNA (Fig. 2C). There were 420 miRNAs detected in mouse plasma and 329 in human plasma. Among them, 178 plasma miRNAs were shared by both mice and humans, accounting for 42% and 54% of mouse and human plasma miRNA, respectively. Among the 329 miRNAs detected in human plasma, 134 miRNAs were upregulated (>1.5-fold) in trauma patients, 28 of which overlapped with the 151 upregulated miRNAs identified in mice with polytrauma. The complete list of plasma miRNAs differentially expressed in both mice and humans after trauma is presented in the heatmaps of Supplemental Fig. 3. The entire RNAseq data were deposited in the NCBI GEO site (GSE223151).

Plasma exRNA in trauma mice triggers proinflammatory cytokine responses in macrophages via TLR7 signaling

To assess the ability of circulating plasma RNA after trauma to induce inflammatory responses, plasma RNA was purified and used to treat BMDMs. We found that plasma exRNA from trauma, but not sham, mice induced robust and dose-dependent (0.175–0.7 μg/ml) IL-6 and MIP-2 production (Fig. 3A). TLR3 and TLR7 are two innate immune receptors sensing dsRNA and ssRNA, respectively

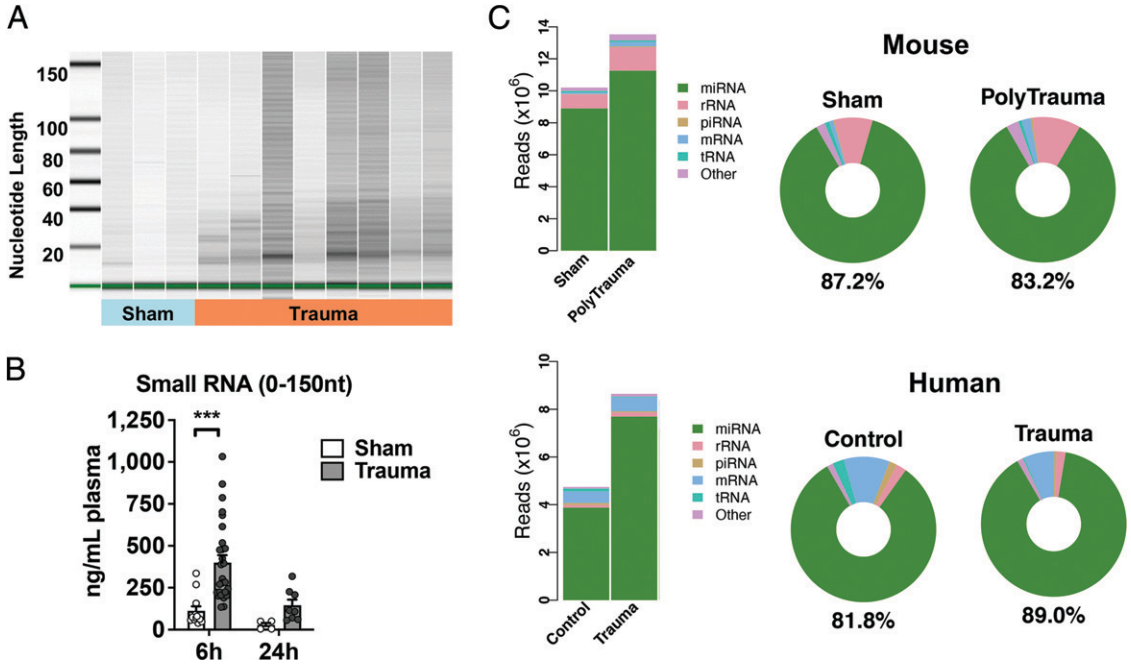

FIGURE 2. Plasma RNA profiling in trauma. (**A**) Capillary electrophoresis analysis of mouse plasma RNA collected at 6 h following sham and trauma procedures. (**B**) Plasma RNA concentrations in sham and septic mice 6 h and 24 h after sham or trauma procedure. ***$p < 0.001$. (**C**) Plasma miRNA profiles of mice and humans. Mouse plasma was collected 6 h after procedures. Human plasma was collected at the time of admission. The bar graphs illustrate the read counts of different plasma RNA biotypes in the plasma. The pie charts represent the different plasma RNA biotypes as percentages. The percentages of miRNA in green color are shown for both mice and humans.

Table I. Demographic and clinical information of the human subjects

	Control (n = 10)	Trauma (n = 10)
Age, y	30.7 (23–37)	32.5 (22–53)
Sex, male	6 (60%)	7 (70%)
Ethnicity		
White	8 (80%)	8 (80%)
Black	1 (10%)	2 (20%)
Mechanism of injury		
MVC		9 (90%)
Fall		1 (10%)
ISS		27.8 (22–49)
Injury characteristics		
Bone fracture		7
Lung injury		4
Splenic injury		4
Liver injury		3
Bowel injury		2
Renal injury		1
Aortic injury		2
Laboratory		
INR		1.51 (0.9–5.4)
PTT, s		25.2 (23–29)
Platelets, $\times 10^3/\mu l$		274.3 (148–426)
Lactate, mmol/L		3.32 (1.9–4.8)

Demographics with average [range] or count (percent).

INR, international normalized ratio; ISS, injury severity score; MVC, motor vehicle crash; PTT, partial thromboplastin time.

(11). As shown in Fig. 3B, trauma plasma exRNAs at the concentration of 0.7 μg/ml induced IL-6 and MIP-2 production in WT BMDMs. Genetic deficiency of TLR7, but not TLR3, significantly attenuated the effect of plasma exRNAs. This marked attenuation of inflammatory responses observed in TLR7-deficient cells appeared specific for exRNA because neither TLR3 nor TLR7 deficiency had any impact on LPS-induced cytokine production, a TLR4-mediated event (Fig. 3B).

Ex-miRNAs identified in trauma mice activate innate immunity via its uridine moieties and TLR7 signaling

To determine the innate immune activity of plasma miRNAs following trauma, we selected 18 miRNAs from the mouse RNAseq data based on the following criteria: (1) ≥1.5-fold upregulated, (2) abundance with >100 read counts, (3) statistically significant (false discovery rate and p value <0.05) in the different expression patterns between sham and trauma mice, and (4) containing various abundance of uridines in their sequences stratified as low (<20% uridine), moderate (≥20 to <40% uridine), and high (≥40% uridine) (Table II), respectively, and tested these miRNA mimics for their abilities to induce IL-6 and MIP-2 production in BMDMs. Among the 18 miRNAs tested, 9 miRNAs (let-7b-5p, let-7j, miR-7a-5p, miR-34a-5p, miR-122-5p, miR-142a-3p, miR-145a-3p, miR-146a-5p, and miR-802-5p) induced dose-dependent cytokine production (Fig. 4A), most with an EC_{50} at submicromolar range, whereas the other 9 miRNAs failed to induce cytokine production (Fig. 4A). Given the critical role of uridine (U) moieties in the binding to the crystal structure of TLR7 by synthetic small ssRNA (31), we performed additional analysis on the four-nucleotide abundance of the tested miRNAs above and their associations with the proinflammatory properties. Compared with the nine noninflammatory miRNAs, the nine proinflammatory miRNAs contained overall more uridines (pro- versus noninflammatory, 40 ± 2% versus 23 ± 2%; $p < 0.001$) (Fig. 4B). In contrast, there was no significant difference in guanosine (G) content between the two groups of miRNAs and a slightly but significantly higher adenosine (A) and cytidine (C) abundance in the noninflammatory group. Moreover, construction of an ROC curve using a binary classification model of "noninflammatory" or "proinflammatory" in an expanded panel of 33 miRNAs (Table III) revealed that the percentage of uridine is the best discriminator of proinflammatory properties with an area under the ROC curve of 0.844 (Fig. 4C). Interestingly, the percentage of adenosine was a similarly good discriminator (area under the ROC curve, 0.769), though appropriately in the opposite sense, given its association with noninflammatory miRNAs, thus representing a strong negative predictor of the immunostimulatory potential of miRNAs. Further experiments revealed that miRNAs with a high percentage of uridine (>40%), such as let-7j, miR-145a-3p, and miR-7a-5p, all induced MIP-2 cytokine and cfB production in WT BMDMs, whereas those with a low percentage of uridine (<20%), such as miR-1947-5p, miR-345-3p, and miR-193b-3p, had minimal or no effect (Fig. 4D, 4E).

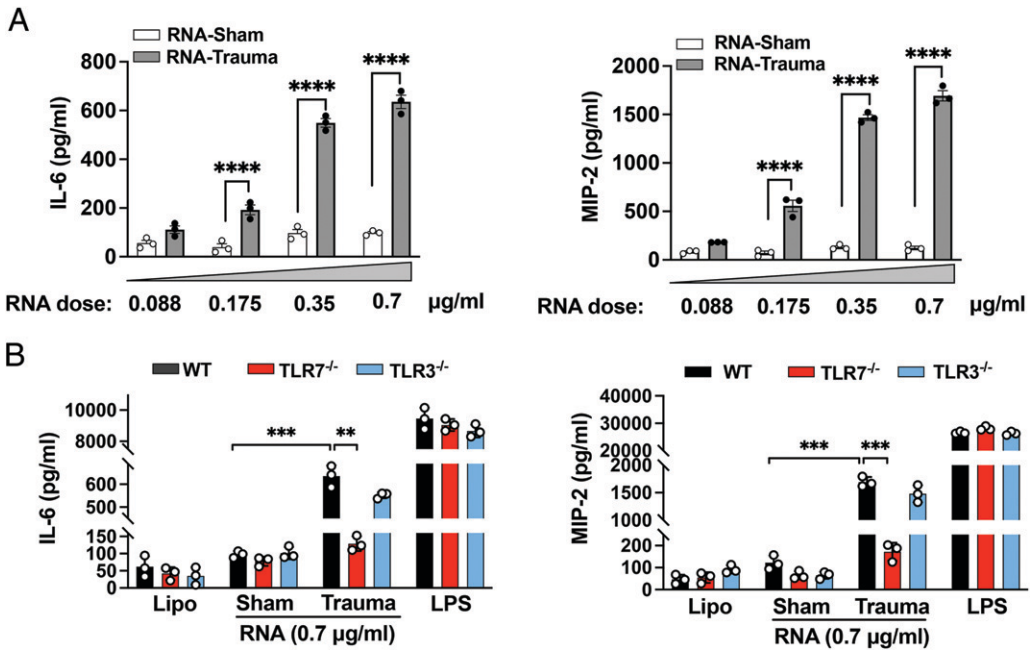

FIGURE 3. Plasma exRNA dose dependently augments cytokine production in cultured macrophages via a TLR7-sensing mechanism. exRNA was isolated from plasma at 6 h after sham or trauma procedure and packed with Lipofectamine (Lipo) prior to the treatment to WT, $TLR7^{-/-}$, and $TLR3^{-/-}$ BMDMs. Media were collected at 18 h, and cytokines were analyzed by ELISA. (**A**) IL-6 and MIP-2 production in WT BMDMs. (**B**) IL-6 and MIP-2 production in WT, $TLR7^{-/-}$, and $TLR3^{-/-}$ BMDMs. Each experiment was independently performed in triplicates and repeated twice. LPS concentration is 100 ng/ml. $^{**}p < 0.01$, $^{***}p < 0.001$, $^{****}p < 0.0001$.

Table II. List of murine miRNAs used in the study and their nucleotide sequences

miRNA	Sequence (5′-3′)	Total No. of Nucleotides	Uridine		Stratified by %U
			No.	%	
let-7j	5′-UGAGGUAUUAGUUUGUGCUGUUAU-3′	24	12	50	High (≥40%)
mir-142a-3p	5′-UGUAGUGUUUCCUACUUUAUGGA-3′	23	11	48	High (≥40%)
mir-7a-5p	5′-UGGAAGACUAGUGAUUUUGUUGU-3′	23	10	43	High (≥40%)
let-7b	5′-UGAGGUAGUAGGUUGUGUGGUU-3′	22	9	41	High (≥40%)
mir-34a-5p	5′-UGGCAGUGUCUUAGCUGGUUGU-3′	22	9	41	High (≥40%)
mir-145a-3p	5′-AUUCCUGGAAAUACUGUUCUUG-3′	22	9	41	High (≥40%)
mir-122-5p	5′-UGGAGUGUGACAAUGGUGUUUG-3′	22	8	36	Moderate (≥20% to <40%)
mir-146a-5p	5′-UGAGAACUGAAUUCCAUGGGUU-3′	22	7	32	Moderate (≥20% to <40%)
mir-802-5p	5′-UCAGUAACAAAGAUUCAUCCUU-3′	22	7	32	Moderate (≥20% to <40%)
mir-451a	5′-AAACCGUUACCAUUACUGAGUU-3′	22	7	32	Moderate (≥20% to <40%)
mir-126a-3p	5′-UCGUACCGUGAGUAAUAAUGCG-3′	22	6	27	Moderate (≥20% to <40%)
mir-374b-5p	5′-AUAUAAUACAACCUGCUAAGUG-3′	22	6	27	Moderate (≥20% to <40%)
mir-192-5p	5′-CUGACCUAUGAAUUGACAGCC-3′	21	5	24	Moderate (≥20% to <40%)
mir-22-3p	5′-AAGCUGCCAGUUGAAGAACUGU-3′	22	5	23	Moderate (≥20% to <40%)
mir-210-3p	5′-CUGUGCGUGUGACAGCGGCUGA-3′	22	5	23	Moderate (≥20% to <40%)
mir-345-3p	5′-CCUGAACUAGGGGUCUGGAGAC-3′	22	4	18	Low (<20%)
mir-1947-5p	5′-AGGACGAGCUAGCUGAGUGCUG-3′	22	4	18	Low (<20%)
mir-193b-3p	5′-AACUGGCCCACAAAGUCCCGCU-3′	22	3	14	Low (<20%)

Single-stranded miRNA mimics are ranked by uridine abundance per miRNA. Uridine % (%U) = No. of uridine/No. of total nucleotides in miRNA × 100%.

Moreover, a series of loss-of-function experiments were designed to determine the necessity of TLR3 or TLR7 in mediating cytokine and cfB production induced by the miRNA mimics and various TLR agonists. As illustrated in Fig. 4F, 4G, cytokine and cfB responses to various miRNA mimics as well as the TLR7 agonist R837 were completely abolished in TLR7$^{-/-}$ but retained in TLR3$^{-/-}$ BMDMs. As expected, MIP-2 and cfB production was attenuated in TLR3$^{-/-}$ cells when stimulated by polyinosinic:polycytidylic acid (TLR3 agonist) but not Pam3cys (TLR2 agonist), suggesting a similar cell condition among different strains. Together, these studies demonstrate that miRNAs with high uridine abundance exhibit greater immunostimulatory effects than those with lower uridine contents, suggesting the importance of uridine nucleotide as a key element in the immune recognition of ex-miRNAs and that the ex-miRNA-induced innate immune activation is entirely TLR7 mediated.

miRNA inhibitors and RNase attenuate the trauma plasma exRNA-induced cytokine production

To determine if the endogenous plasma exRNA-induced cytokine production in trauma was attributed to miRNAs, we treated exRNA extracted from sham and trauma animals with anti-miRs specifically against the proinflammatory miRNAs: miR-7a, miR-142a, let7j, miR-802, and miR-146a, as identified above. As noted in Fig. 5A, these individual miRNA inhibitors blocked at various degrees the plasma exRNA-induced IL-6 and MIP-2 production in BMDMs. Importantly, pretreatment with RNase but not DNase of plasma exRNAs completely abolished the cytokine production in trauma exRNA-treated BMDMs (Fig. 5B).

TLR7-knockout mice are protected against trauma-induced inflammation and lung injury

Given the role of TLR7 in plasma exRNA sensing and their innate immune activities, we next tested the necessity of TLR7 in mediating systemic inflammation and organ injury in a murine model of polytrauma. As shown in Fig. 6A, compared with WT mice, age- and sex-matched TLR7-knockout (KO) mice had significantly lower IL-6 and MIP-2 levels in the plasma 6 h after polytrauma. Moreover, the BAL levels of the proinflammatory cytokines were significantly lower in TLR7-KO mice following trauma (Fig. 6B). TLR7$^{-/-}$ also had less severe liver injury, as evidenced by lower plasma AST levels (Fig. 6C). Moreover, there was a trend, albeit statistically insignificant, toward better survival in TLR7-KO mice after day 3 of traumatic injury (Fig. 6D). However, and somewhat surprisingly, although WT mice developed significant cardiac dysfunction 6 h after polytrauma as assessed by echocardiography with decreased ejection fraction and fractional shortening, decreased stroke volumes, and CO, TLR7-KO mice exhibited no sign of improvement with similar levels of cardiac dysfunction at 6 h (Fig. 6E).

Discussion

In this study, we established a mouse model of polytrauma that models clinical trauma patients with systemic inflammation and multiple organ injury. We found that hours after traumatic insults, there was a marked increase in plasma exRNAs in both mice and humans. Moreover, endogenous plasma RNA isolated from trauma mice, but not that of sham control, was capable of inducing a dose-dependent proinflammatory cytokine production in immune cells in a TLR7-dependent manner. RNAseq profiling of plasma RNA identified markedly differential expression of a large group of plasma miRNAs between trauma and control in both mice and humans. Bioinformatic analysis and in vitro testing of a group of miRNA mimics selected from the plasma RNAseq data have indicated the importance of uridine abundance in predicting the proinflammatory property of miRNA molecules. Loss-of-function studies employing miRNA inhibitors and TLR7-KO mice demonstrated the important role of miRNA-TLR7 signaling in mediating proinflammatory effects of exRNA in vitro. Finally, TLR7$^{-/-}$ mice appeared to be protected in part from polytrauma-induced systemic inflammation and organ injury.

The polytrauma model in our study was designed to simulate blast injury to the low extremities (bone and muscle) and abdomen (bowel) caused by improvised explosive devices that often occurred during the recent U.S. Middle East conflict. In addition to muscle and bone injury to the extremities from direct exposure to high-energy explosives and fragmentation, survivors of blast injuries often present with nonpenetrating injury to hollow viscera, including ischemic injury from either hypotension and/or direct disruption of mesenteric vessels and tissues resulting from blast overpressure waves that propagate through the abdominal wall and solid organs (32). It is worth noting that although severe trauma often involves

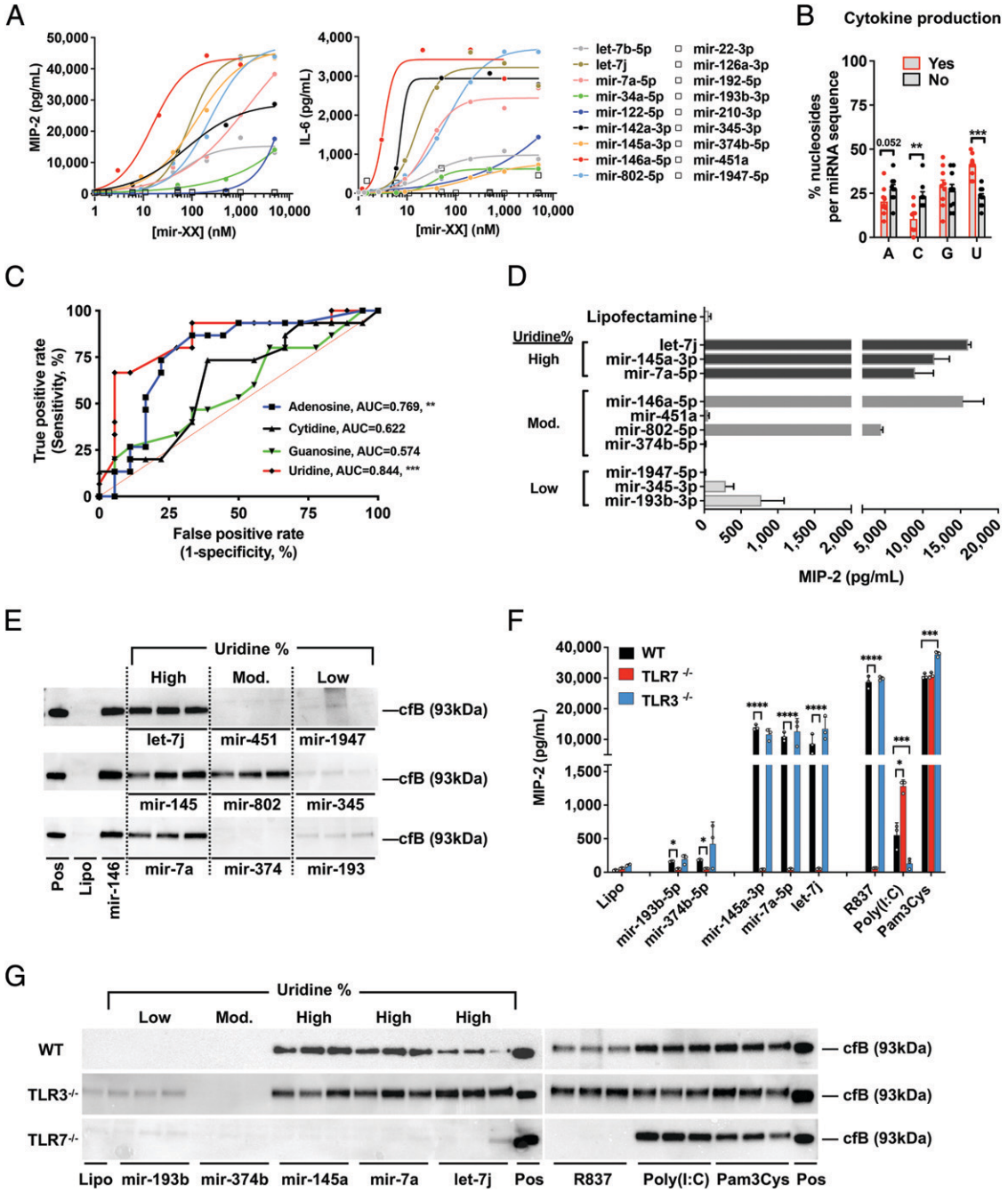

FIGURE 4. High uridine abundance is associated with the proinflammatory properties of miRNAs. (**A**) Dose–response curve of miRNA-induced IL-6 and MIP-2 production. (**B**) Comparison of nucleotide (A, C, G, U) abundance in pro- and noninflammatory miRNAs. $n = 9$/group. $^{**}p < 0.01$, $^{***}p < 0.001$. (**C**) ROC curves of nucleotide (A, C, G, U) abundance to predict proinflammatory property of miRNAs. (**D** and **E**) Effect of miRNA mimics with different uridine abundances (high, moderate, low) on MIP-2 (D) and cfB (E) production in BMDMs. (**F** and **G**) miRNA-induced MIP-2 (F) and cfB (G) production in WT and TLR3$^{-/-}$ cells, but not in TLR7$^{-/-}$ BMDMs. Reagent concentrations used in (D–G): miRNA mimics, 50 nM; R837, 1 μg/ml; polyinosinic:polycytidylic acid, 10 μg/ml; Pam3cys, 1 μg/ml. Lipo, Lipofectamine; Pos, WT plasma serving as positive control for cfB. $^{*}p < 0.05$, $^{***}p < 0.001$, $^{****}p < 0.0001$. Each experiment was independently performed in triplicate and repeated twice.

significant hemorrhage and hypovolemia, a main cause of early trauma mortality, many trauma patients sustain severe injuries without associated hemorrhagic shock. These may include multiple soft tissue and bony injuries, such as the blunt trauma with bone fracture, muscle crush, and nonpenetrating chest and abdominal organ injury. Thus, our polytrauma model achieved the goal of approximating these clinical situations using a combination of bowel ischemia, long bone fracture, and tissue injury. The polytrauma model mimics the clinical state of hypothermia; direct local organ injury; and, importantly, multiple remote organ injury to the lung, heart, kidney, and liver. Moreover, the polytrauma model generated a massive acute inflammatory response, reflecting the expected course of innate immune activation following a single traumatic insult. However, given the heterogeneous nature of injuries, such as bone fracture, muscle crush, and bowel ischemia, it is difficult to link systemic effects and organ injuries to one particular insult, which can be viewed as a limitation of the model from a mechanistic standpoint.

Table III. Binary classification schemata for miRNAs used in percentage uridine analyses

miRNA	Uridine (%)	Inflammatory?	miRNA	Uridine (%)	Inflammatory?
let-7j	50	Yes	mir-499-5p	43	No
mir-142a-3p	48	Yes	mir-144-3p	35	No
mir-7a-5p	43	Yes	mir-144-5p	35	No
mir-145a-3p	41	Yes	mir-451-a	32	No
let-7b	41	Yes	mir-1a-3p	32	No
mir-34a-5p	41	Yes	mir-374b-5p	27	No
mir-181d-5p	39	Yes	mir-126a-3p	27	No
mir-215-3p	38	Yes	mir-150-5p	27	No
mir-122-5p	36	Yes	mir-26a-5p	27	No
mir-186-5p	36	Yes	mir-192-5p	24	No
mir-25-3p	36	Yes	mir-210-3p	23	No
mir-382-5p	36	Yes	mir-22-3p	23	No
mir-26b-5p	33	Yes	mir-345-3p	18	No
mir-802-5p	32	Yes	mir-1947-5p	18	No
mir-145a-5p	32	Yes	mir-193b-3p	14	No
mir-133a-3p	32	Yes			
mir-146a-5p	30	Yes			
mir-208a-3p	18	Yes			
		$n = 18$			$n = 15$

Synthetic ss-miRNAs, rank list ordered by percentage uridine below, were tested at effective doses of 50 nM in BMDM culture. miRNAs capable of inducing both MIP-2 and IL-6 were classified as inflammatory (left, $n = 18$), whereas the absence of a cytokine response was classified as noninflammatory (right, $n = 15$). Uridine % = No. of uridine/No. of total nucleotides × 100%.

To our knowledge, one of the novel findings in the current study was the proinflammatory property of plasma RNA in trauma mice. The fact that the same amount of plasma RNA from sham mice failed to achieve the effect suggests that traumatic injury may have altered the plasma RNA profiles such that it possesses proinflammatory characteristics. Indeed, the unbiased RNAseq analysis demonstrated a differential expression pattern of multiple plasma miRNAs between trauma and health in both mice and humans, and that ex-miRNAs represent the most predominant exRNA biotype in the plasma. Moreover, there is substantial overlap in plasma miRNAs between mice and humans. These observations are consistent with other studies that have documented the roles of circulating miRNAs as potential circulating biomarkers for defining various disease states such as myocardial infarction (33, 34), systemic inflammatory response syndrome (35), and sepsis (36, 37). For example, in a study of experimental sepsis induced by cecal ligation and puncture, levels of many miRNAs, such as miR-145-5p, miR-122-5p, miR-146a-5p, miR-34a-5p, and miR-210-3p, are clearly elevated in septic mice compared with control animals (21, 22), suggesting that expression profiles of miRNAs are potential indicators of an increasingly complex pathology. Similarly, patterns of miRNA differential expression have been studied in severely injured patients, suggesting potential correlations between miRNAs and key clinical outcomes, such as acidosis, coagulopathy, and transfusion requirements (18, 21, 22). However, mere observations about the relative presence of individual miRNA patterns provide little information in terms of direct evidence on the specific function of miRNAs and how they may initiate or perpetuate the complex postinjury inflammation and contribute to trauma-induced downstream pathogenesis. Finally, it should be pointed out that although both male and female human subjects were enrolled, only male mice were used for the plasma RNAseq profiling and other experiments in the present study, which represents a major limitation. There are ample studies in animals and humans that demonstrate sex differences in trauma pathophysiology, posttraumatic recovery, and treatment efficacy (38–41).

Our efforts to identify the unique role of miRNAs in regulating the inflammatory response in trauma stems from prior observations

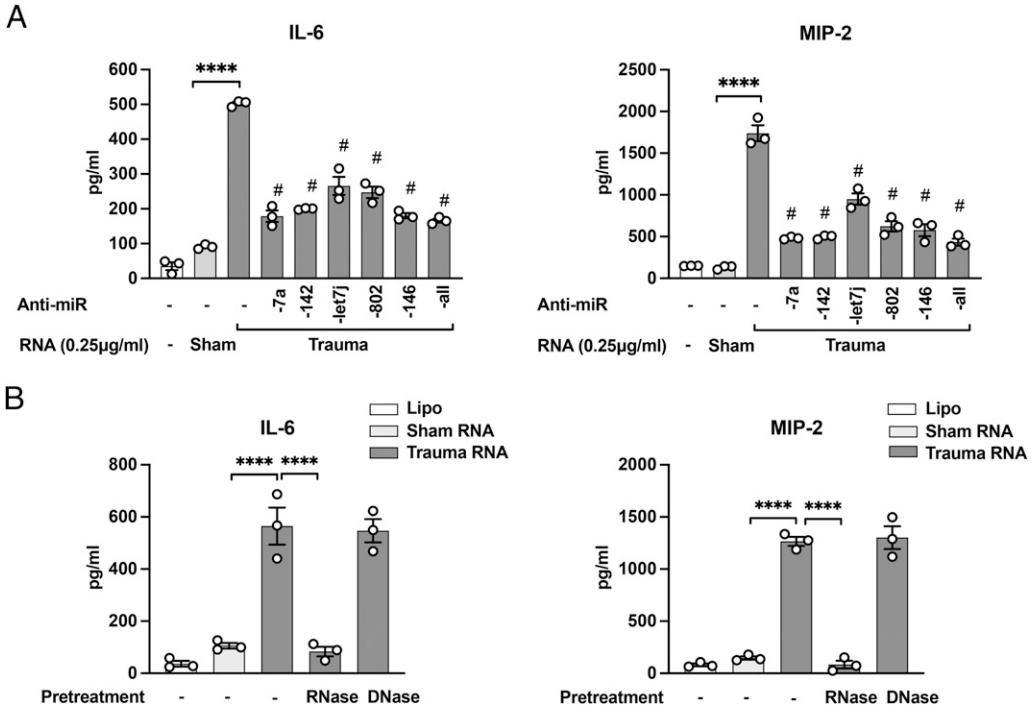

FIGURE 5. Effect of anti-miRNAs and RNase on plasma exRNA-induced cytokine production in macrophages. (**A**) Effect of anti-miRNAs on plasma exRNA-induced IL-6 and MIP-2 production. BMDMs were pretreated with or without anti-miR at 50 nM each or a combination of all five anti-miRs at 250 nM for 1 h and then treated with Lipofectamine-packed plasma exRNA at 0.25 μg/ml for 18 h. Cytokines were analyzed by ELISA. ****$p < 0.0001$, $^{\#}p < 0.01$ versus trauma RNA treatment without anti-miR inhibitors. Each experiment was independently performed in triplicate and repeated twice. (**B**) Effect of RNase and DNase on plasma RNA-induced IL-6 and MIP-2 production. RNA (0.25 μg/ml) from sham or trauma plasma was incubated with RNase (10 μg) or DNase (1 U) at room temperature for 30 min before being packed with Lipofectamine (Lipo) to treat BMDMs. Media were collected at 18 h for ELISA analysis of cytokine. ****$p < 0.0001$. Each experiment was independently performed in triplicate and repeated twice.

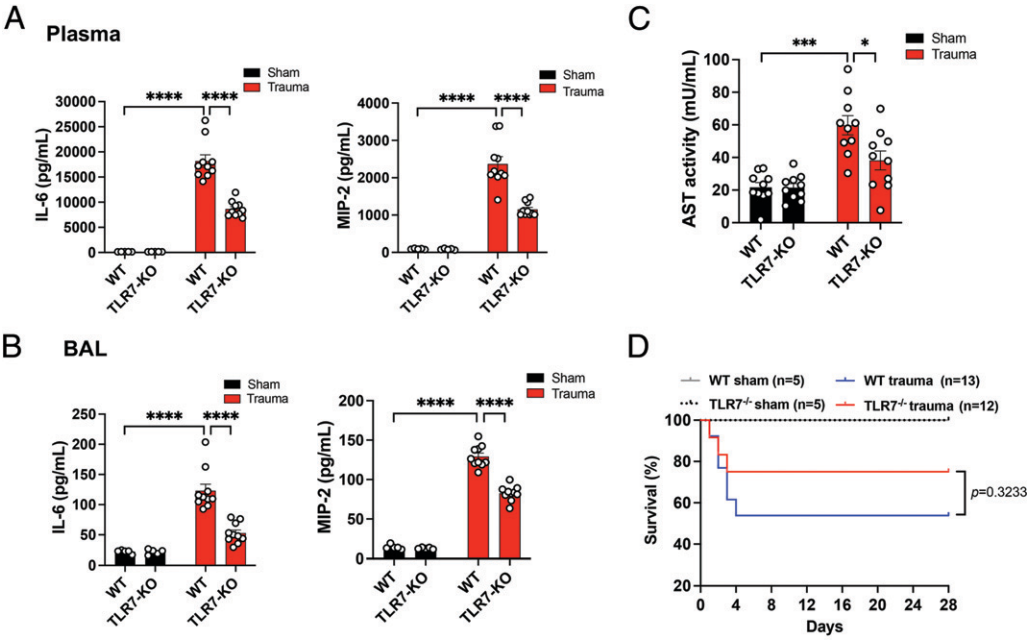

FIGURE 6. Absence of TLR7 attenuates polytrauma-induced systemic and lung inflammation and mitigates liver injury. WT and TLR7-KO mice were subjected to sham or polytrauma procedures. (**A**–**C**) Mice were euthanized, and samples were collected at 6 h after sham or trauma procedures to test plasma cytokines (A), BAL cytokines (B), and liver AST activity (C). Each data point represents a mouse. $*p < 0.05$, $***p < 0.001$, $****p < 0.0001$. (**D**) Survival rate after sham and trauma mice. Animal number in each group is indicated in the figure legend. Of note, one mouse in the TLR7$^{-/-}$ trauma group was lost postoperatively in the vivarium facility. (**E**) Mouse cardiac function by echocardiography. Each data point represents an animal subject. $n = 5$ in sham group, $n = 10$ in trauma group. p 1, WT-sham versus WT trauma; p 2, KO-sham versus KO trauma; p 3, WT trauma versus KO trauma.

E **Echocardiographic measurements before and after trauma in WT and TLR7 KO mice**

Group: (n)	WT-Sham (5)	TLR7 KO-Sham (5)	WT-Trauma (10)	TLR7 KO-Trauma (10)	*p* 1	*p* 2	*p* 3
Baseline							
HR, bpm	649±21	666±6	665±9	668±16	ns	ns	ns
FS, %	50.0±1.2	47.4±1.8	49.1±0.6	47.8±1.2	ns	ns	ns
EF, %	82.8±1.2	80.0±1.4	81.8±0.6	80.6±1.2	ns	ns	ns
CO, ml/min	18.6±0.9	17.6±0.6	17.5±0.6	16.9±0.9	ns	ns	ns
SV, µl	28.7±1.2	25.3±0.7	26.3±0.7	25.2±1.1	ns	ns	ns
6h Post-surgery							
HR, bpm	662±13	663±9	480±26	390±35	<0.001	<0.0001	ns
FS, %	47.6±1.3	48.4±2.2	34.1±3.3	33.4±2.6	<0.05	<0.05	ns
EF, %	79.6±1.7	81.0±1.9	64.0±4.4	63.9±3.5	ns	<0.05	ns
CO, ml/min	23.7±1.9	19.8±0.8	7.3±1.6	5.4±1.4	<0.0001	<0.0001	ns
SV, µl	35.8±3.0	29.8±0.9	14.3±2.5	12.7±2.2	<0.0001	<0.0001	ns

that certain miRNAs have a unique property of triggering innate immune responses in various cells (macrophages, microglia, astrocytes, and cardiomyocytes) and organs (the brain, lung, and heart), such as cytokine or complement factor production and innate immune cell activation (12, 21, 24, 42). Furthermore, we have previously demonstrated that systemic administration of RNase or nucleic acid–binding nanoprobes reduces ischemic myocardial injury (33, 43) and that genetic deletion of TLR7 improves sepsis outcomes (24, 25, 44–46), further supporting the concept that exRNA sensing via TLR7 is a key proinflammatory driver under certain inflammatory conditions.

Our bioinformatic analysis and cytokine/cfB testing of various miRNA mimics revealed the importance of uridine abundance in miRNA molecules in their proinflammatory properties. Among the miRNA mimics tested in the study, those with high uridine abundance (>40%) have greater immunostimulatory effects than the ones with lower uridine contents (<20%). The molecular explanation behind these observations is probably due to the critical role of uridine in ssRNA binding to TLR7. In a structural analysis of TLR7, Zhang and colleagues demonstrated that one of the two nucleotide binding sites in the crystal structures of TLR7 specifically binds to uridine moieties in ssRNA and that successive uridine-containing ssRNAs have full binding capability to TLR7 (31, 47). Along the same line, we recently analyzed the nucleotide sequences of a group of 33 miRNAs, both proinflammatory and noninflammatory. Using a computer exhaustive search algorithm, we identified UU…U as the functional motif of the proinflammatory miRNAs, which was further validated experimentally in vitro via a series of single U→A mutations and cytokine testing with miR-146a-5p (22).

The in vivo loss-of-function study in TLR-KO mice demonstrated an essential role of TLR7 signaling in trauma-induced systemic inflammation and the downstream pathogenesis of multiple organ injury following traumatic insult. Additional studies using pharmacological antagonists to TLR7 signaling will be needed to validate these findings. However, the fact that TLR7-KO mice were only partially protected with attenuated systemic inflammation and organ injuries suggests that different endogenous danger receptor systems may also play a role (8).

In summary, in a murine model of polytrauma, we demonstrate a unique proinflammatory property of plasma RNA. RNAseq analysis reveals a marked differential expression of a large group of plasma miRNAs in both mice and humans following severe traumatic injury. Mechanistically, our study demonstrates that trauma plasma exRNA and certain ex-miRNAs with high uridine abundance elicit their proinflammatory effects via TLR7 signaling. Compared with WT mice, mice with genetic deletion of TLR7 have attenuated inflammation and

organ injury following polytrauma. These data establish an important role of exRNA-TLR7 signaling in trauma-induced inflammation and organ injury.

Acknowledgments

We thank Ashely Cellini from Pathology Biorepository Shared Services, University of Maryland School of Medicine, for assistance with histology. We thank Jessica Neder for the preparation of bone marrow-derived macrophages.

Disclosures

The authors have no financial conflicts of interest.

References

1. Tremoleda, J. L., S. A. Watts, P. S. Reynolds, C. Thiemermann, and K. Brohi. 2017. Modeling acute traumatic hemorrhagic shock injury: challenges and guidelines for preclinical studies. *Shock* 48: 610–623.
2. Rhee, P., B. Joseph, V. Pandit, H. Aziz, G. Vercruysse, N. Kulvatunyou, and R. S. Friese. 2014. Increasing trauma deaths in the United States. *Ann. Surg.* 260: 13–21.
3. A Guide to U.S. Military Casualty Statistics: Operation Freedom's Sentinel, Operation Inherent Resolve, Operation New Dawn, Operation Iraqi Freedom, and Operation Enduring Freedom. Available at: https://crsreports.congress.gov/product/pdf/RS/RS22452.
4. Keel, M., and O. Trentz. 2005. Pathophysiology of polytrauma. *Injury* 36: 691–709.
5. Jagodzinski, N. A., C. Weerasinghe, and K. Porter. 2010. Crush injuries and crush syndrome - a review. Part 2: the local injury. *Trauma* 12: 133–148.
6. Simmons, J. W., and M. F. Powell. 2016. Acute traumatic coagulopathy: pathophysiology and resuscitation. *Br. J. Anaesth.* 117(suppl 3): iii31–iii43.
7. Lord, J. M., M. J. Midwinter, Y. F. Chen, A. Belli, K. Brohi, E. J. Kovacs, L. Koenderman, P. Kubes, and R. J. Lilford. 2014. The systemic immune response to trauma: an overview of pathophysiology and treatment. *Lancet* 384: 1455–1465.
8. Huber-Lang, M., J. D. Lambris, and P. A. Ward. 2018. Innate immune responses to trauma. *Nat. Immunol.* 19: 327–341.
9. Moore, E. E., H. B. Moore, L. Z. Kornblith, M. D. Neal, M. Hoffman, N. J. Mutch, H. Schöchl, B. J. Hunt, and A. Sauaia. 2021. Trauma-induced coagulopathy. [Published erratum appears in 2022 *Nat. Rev. Dis. Primers* 8: 25.] *Nat. Rev. Dis. Primers* 7: 30.
10. Kawai, T., and S. Akira. 2010. The role of pattern-recognition receptors in innate immunity: update on Toll-like receptors. *Nat. Immunol.* 11: 373–384.
11. Roers, A., B. Hiller, and V. Hornung. 2016. Recognition of endogenous nucleic acids by the innate immune system. *Immunity* 44: 739–754.
12. Chen, F., L. Zou, B. Williams, and W. Chao. 2021. Targeting Toll-like receptors in sepsis: from bench to clinical trials. *Antioxid. Redox Signal.* 35: 1324–1339.
13. Diebold, S. S., T. Kaisho, H. Hemmi, S. Akira, and C. Reis e Sousa. 2004. Innate antiviral responses by means of TLR7-mediated recognition of single-stranded RNA. *Science* 303: 1529–1531.
14. Sioud, M. 2005. Induction of inflammatory cytokines and interferon responses by double-stranded and single-stranded siRNAs is sequence-dependent and requires endosomal localization. *J. Mol. Biol.* 348: 1079–1090.
15. Miyake, K., T. Shibata, U. Ohto, T. Shimizu, S. I. Saitoh, R. Fukui, and Y. Murakami. 2018. Mechanisms controlling nucleic acid-sensing Toll-like receptors. *Int. Immunol.* 30: 43–51.
16. Zhang, Q., M. Raoof, Y. Chen, Y. Sumi, T. Sursal, W. Junger, K. Brohi, K. Itagaki, and C. J. Hauser. 2010. Circulating mitochondrial DAMPs cause inflammatory responses to injury. *Nature* 464: 104–107.
17. Yang, J., H. Han, Y. Zhao, and H. Qin. 2015. Specific miRNA and its target in neutrophils after traumatic injury. *Acta Biochim. Biophys. Sin. (Shanghai)* 47: 749–754.
18. Uhlich, R. M., J. A. Konie, J. W. Davis, M. L. Misfeldt, C. Nelson, R. Calaluce, and S. L. Barnes. 2014. Novel microRNA correlations in the severely injured. *Surgery* 156: 834–841.
19. Bedreag, O. H., A. F. Rogobete, R. Dumache, M. Sarandan, A. C. Cradigati, M. Papurica, M. C. Craciunescu, D. M. Popa, L. Luca, R. Nartita, and D. Sandesc. 2015. Use of circulating microRNAs as biomarkers in critically ill polytrauma patients. *Biomarkers Genomic Med.* 7: 131–138.
20. Yeri, A., A. Courtright, R. Reiman, E. Carlson, T. Beecroft, A. Janss, A. Siniard, R. Richholt, C. Balak, J. Rozowsky, et al. 2017. Total extracellular small RNA profiles from plasma, saliva, and urine of healthy subjects. *Sci. Rep.* 7: 44061.
21. Zou, L., Y. Feng, G. Xu, W. Jian, and W. Chao. 2016. Splenic RNA and MicroRNA mimics promote complement factor B production and alternative pathway activation via innate immune signaling. *J. Immunol.* 196: 2788–2798.
22. Wang, S., Y. Yang, A. Suen, J. Zhu, B. Williams, J. Hu, F. Chen, R. Kozar, S. Shen, Z. Li, et al. 2021. Role of extracellular microRNA-146a-5p in host innate immunity and bacterial sepsis. *iScience* 24: 103441.
23. Feng, Y., L. Zou, D. Yan, H. Chen, G. Xu, W. Jian, P. Cui, and W. Chao. 2017. Extracellular microRNAs induce potent innate immune responses via TLR7/MyD88-dependent mechanisms. *J. Immunol.* 199: 2106–2117.
24. Huang, H., J. Zhu, L. Gu, J. Hu, X. Feng, W. Huang, S. Wang, Y. Yang, P. Cui, S. H. Lin, et al. 2022. TLR7 mediates acute respiratory distress syndrome in sepsis by sensing extracellular miR-146a. *Am. J. Respir. Cell Mol. Biol.* 67: 375–388.
25. Zou, L., J. He, L. Gu, R. A. Shahror, Y. Li, T. Cao, S. Wang, J. Zhu, H. Huang, F. Chen, et al. 2022. Brain innate immune response via miRNA-TLR7 sensing in polymicrobial sepsis. *Brain Behav. Immun.* 100: 10–24.
26. Robinson, M. D., D. J. McCarthy, and G. K. Smyth. 2010. edgeR: a Bioconductor package for differential expression analysis of digital gene expression data. *Bioinformatics* 26: 139–140.
27. Kolde, R., and J. Vilo. 2015. GOsummaries: an R package for visual functional annotation of experimental data. *F1000 Res.* 4: 574.
28. Ru, Y., K. J. Kechris, B. Tabakoff, P. Hoffman, R. A. Radcliffe, R. Bowler, S. Mahaffey, S. Rossi, G. A. Calin, L. Bemis, and D. Theodorescu. 2014. The multiMiR R package and database: integration of microRNA-target interactions along with their disease and drug associations. *Nucleic Acids Res.* 42: e133.
29. Yu, G., L. G. Wang, Y. Han, and Q. Y. He. 2012. clusterProfiler: an R package for comparing biological themes among gene clusters. *OMICS* 16: 284–287.
30. Zou, L., Y. Feng, Y. Li, M. Zhang, C. Chen, J. Cai, Y. Gong, L. Wang, J. M. Thurman, X. Wu, et al. 2013. Complement factor B is the downstream effector of TLRs and plays an important role in a mouse model of severe sepsis. *J. Immunol.* 191: 5625–5635.
31. Zhang, Z., U. Ohto, T. Shibata, E. Krayukhina, M. Taoka, Y. Yamauchi, H. Tanji, T. Isobe, S. Uchiyama, K. Miyake, and T. Shimizu. 2016. Structural analysis reveals that Toll-like receptor 7 is a dual receptor for guanosine and single-stranded RNA. *Immunity* 45: 737–748.
32. Turégano-Fuentes, F., D. Pérez-Diaz, M. Sanz-Sánchez, R. Alfici, and I. Ashkenazi. 2014. Abdominal blast injuries: different patterns, severity, management, and prognosis according to the main mechanism of injury. *Eur. J. Trauma Emerg. Surg.* 40: 451–460.
33. Chen, C., Y. Feng, L. Zou, L. Wang, H. H. Chen, J. Y. Cai, J. M. Xu, D. E. Sosnovik, and W. Chao. 2014. Role of extracellular RNA and TLR3-Trif signaling in myocardial ischemia-reperfusion injury. *J. Am. Heart Assoc.* 3: e000683.
34. Feng, Y., H. Chen, J. Cai, L. Zou, D. Yan, G. Xu, D. Li, and W. Chao. 2015. Cardiac RNA induces inflammatory responses in cardiomyocytes and immune cells via Toll-like receptor 7 signaling. *J. Biol. Chem.* 290: 26688–26698.
35. Caserta, S., F. Kern, J. Cohen, S. Drage, S. F. Newbury, and M. J. Llewelyn. 2016. Circulating plasma microRNAs can differentiate human sepsis and systemic inflammatory response syndrome (SIRS). *Sci. Rep.* 6: 28006.
36. Vasilescu, C., M. Dragomir, M. Tanase, D. Giza, R. Purnichescu-Purtan, M. Chen, S. J. Yeung, and G. A. Calin. 2017. Circulating miRNAs in sepsis—a network under attack: an in-silico prediction of the potential existence of miRNA sponges in sepsis. *PLoS One* 12: e0183334.
37. Essandoh, K., and G. C. Fan. 2014. Role of extracellular and intracellular microRNAs in sepsis. *Biochim. Biophys. Acta* 1842: 2155–2162.
38. Starkey, N. J., B. Duffy, K. Jones, A. Theadom, S. Barker-Collo, and V. Feigin; BIONIC8 Research Group. 2022. Sex differences in outcomes from mild traumatic brain injury eight years post-injury. *PLoS One* 17: e0269101.
39. Mollayeva, T., S. Mollayeva, and A. Colantonio. 2018. Traumatic brain injury: sex, gender and intersecting vulnerabilities. *Nat. Rev. Neurol.* 14: 711–722.
40. Gupte, R., W. Brooks, R. Vukas, J. Pierce, and J. Harris. 2019. Sex differences in traumatic brain injury: what we know and what we should know. *J. Neurotrauma* 36: 3063–3091.
41. Gölz, C., F. P. Kirchhoff, J. Westerhorstmann, M. Schmidt, T. Hirnet, G. M. Rune, R. A. Bender, and M. K. E. Schäfer. 2019. Sex hormones modulate pathogenic processes in experimental traumatic brain injury. *J. Neurochem.* 150: 173–187.
42. Shimada, B. K., Y. Yang, J. Zhu, S. Wang, A. Suen, S. M. Kronstadt, A. Jeyaram, S. M. Jay, L. Zou, and W. Chao. 2020. Extracellular miR-146a-5p induces cardiac innate immune response and cardiomyocyte dysfunction. *Immunohorizons* 4: 561–572.
43. Chen, H. H., H. Yuan, H. Cho, Y. Feng, S. Ngoy, A. T. Kumar, R. Liao, W. Chao, L. Josephson, and D. E. Sosnovik. 2017. Theranostic nucleic acid binding nanoprobe exerts anti-inflammatory and cytoprotective effects in ischemic injury. *Theranostics* 7: 814–825.
44. Jian, W., L. Gu, B. Williams, Y. Feng, W. Chao, and L. Zou. 2019. Toll-like receptor 7 contributes to inflammation, organ injury, and mortality in murine sepsis. *Anesthesiology* 131: 105–118.
45. Williams, B., J. Neder, P. Cui, A. Suen, K. Tanaka, L. Zou, and W. Chao. 2019. Toll-like receptors 2 and 7 mediate coagulation activation and coagulopathy in murine sepsis. *J. Thromb. Haemost.* 17: 1683–1693.
46. Williams, B., J. Zhu, L. Zou, and W. Chao. 2022. Innate immune TLR7 signaling mediates platelet activation and platelet-leukocyte aggregate formation in murine bacterial sepsis. *Platelets* 33: 1251–1259.
47. Zhang, Z., U. Ohto, T. Shibata, M. Taoka, Y. Yamauchi, R. Sato, N. M. Shukla, S. A. David, T. Isobe, K. Miyake, and T. Shimizu. 2018. Structural analyses of Toll-like receptor 7 reveal detailed RNA sequence specificity and recognition mechanism of agonistic ligands. *Cell Rep.* 25: 3371–3381.e5.